Multiscale Part-Spectrum *k*-Distribution Database for Atomic Radiation in Hypersonic Nonequilibrium Flows

Ankit Bansal
Department of Mechanical Engineering,
The Pennsylvania State University,
University Park, PA 16802,
e-mail: azb162@psu.edu

Michael Modest[1]
Fellow ASME
School of Engineering,
University of California, Merced,
Merced, CA 95343
e-mail: MModest@eng.ucmerced.edu

An accurate and compact part-spectrum k*-distribution database has been developed for the two most important radiating species N and O encountered in hypersonic nonequilibrium flows. The database allows users to calculate the desired full-spectrum* k*-distributions through look-up and interpolation, providing an efficient means to perform radiative transfer calculations. A detailed methodology of the* k*-distribution data generation is presented. An optimized Gauss quadrature scheme is implemented for reducing the size of the database. The accuracy of the database is determined by comparing part-spectrum emissivities with those obtained from line-by-line calculations. The application of the database to construct full-spectrum* k*-distributions at arbitrary gas states is discussed. Heat transfer results for the stagnation line of the Stardust vehicle are discussed and CPU-time studies are presented, demonstrating the accuracy and efficiency of the* k*-distribution database.* [DOI: 10.1115/1.4004528]

Keywords: hypersonic, radiation, nonequilibrium, k-distribution

1 Introduction

An accurate and efficient modeling of radiative heat transfer is necessary for optimal design of new generation space vehicles. In high-temperature plasma encountered during atmospheric entry of spacecrafts, the flow is highly dissociated, and radiation from atomic species, including bound–bound and continuum radiation, is a major source of heat transfer to the space vehicle. The strong spectral structure of atomic radiation requires a line-by-line (LBL) solution of the radiative transfer equation (RTE) at several hundred thousand wavelengths, making it extremely expensive to solve when coupled with a flow solver.

It has been shown that, for a small spectral interval in a homogeneous medium, the absorption coefficients can be reordered into a monotonic *k*-distribution, which yields exact results at a fraction of the computational cost required by line-by-line methods [1]. Modest and Zhang extended the *k*-distribution concept to the full spectrum, calling it the full-spectrum *k*-distribution method (FSK), and also to inhomogeneous media [2,3]. While the *k*-distribution method is exact for a homogeneous medium, significant errors may occur when applied to strongly inhomogeneous media. Over the years, a number of new adaptations of the *k*-distribution method have evolved. The problem of inhomogeneity is addressed by using one of two different approaches: the scaling approximation or the assumption of a correlated *k*-distribution [3]. Both the scaled and correlated-*k* approaches may result in significant errors when dealing with inhomogeneous media because neither the scaled nor the correlated assumptions are ever truly accurate. The resulting errors and the applicability of scaled and correlated-*k* method have been discussed by Modest [3].

It was recognized [4,5] that, in high-temperature combustion applications, at significantly different temperatures different spectral lines dominate the radiative transfer, and the assumption of a correlated absorption coefficient breaks down. Similarly, in a mixture of gases, the correlation breaks down in the presence of strong concentration gradients, as recognized by Modest and Zhang [2]. To overcome some of these difficulties, Modest and Zhang developed the multiscale full-spectrum correlated-*k* distribution method (MSFSCK) [6], in which different lines are placed into separate "scales" based on their temperature dependence, and the multigroup full-spectrum correlated-*k* distribution method (MGFSCK) [7], where different spectral positions are placed into the different spectral groups according to their temperature and pressure dependence. The multigroup model has the advantage that it avoids the problem of overlap between the spectral groups but is not trivial to apply to gas mixtures. In contrast, in the MSFSCK method, the approximate treatment of overlap between different scales may lead to additional inaccuracy.

In the field of atomic line radiation, the reordering concept was introduced by Hermann and Schade [8] for high-temperature cylindrical nitrogen arcs. This model is very similar to the part-spectrum based approach used in this work. Recently, Bansal et al. [9] have developed a MGFSCK method for radiation transfer in hypersonic nonequilibrium flows, containing the strongly radiating atomic species of N and O. The shock layer of a reentry space vehicle is marked by the presence of extreme temperature and concentration gradients. The nonequilibrium flow-field cannot be represented by a single temperature, and the radiation field is governed by a number of collisional processes. Bansal et al. have discussed the various challenges posed by these extreme conditions.

While FSCK and MGFSCK approaches make it possible to evaluate the radiative fluxes at a fraction of the cost needed by line-by-line methods, considerable preparatory work is required before the methods can be used: (i) determination of the spectral absorption coefficient for all flow conditions, and (ii) assembly of *k*-distributions from the absorption coefficients. It is advantageous to database *k*-distributions, from which any desired full-spectrum *k*-distribution can be calculated on-the-fly. Modest and Riazzi [10] have shown the advantages and applicability of using such a database in combustion applications. They databased a set of *k*-distributions as a function of thermodynamic state parameters. The databasing scheme was further optimized by Wang and Modest [11], who demonstrated the use of various quadrature schemes for preparing a highly accurate and compact database.

[1]Corresponding author.

Contributed by the Heat Transfer Division of ASME for publication in the JOURNAL OF HEAT TRANSFER. Manuscript received July 24, 2010; final manuscript received June 27, 2011; published online October 7, 2011. Assoc. Editor: Walter W. Yuen.

In the case of nonequilibrium atomic radiation, there are a large number of parameters to database, which include translation and electron temperatures and number densities of electrons, neutral atoms, and ions. The presence of such a large number of parameters complicates the databasing scheme. However, some of these difficulties can be overcome by appropriately dividing the full spectrum into a number of part spectra. This paper is an improvement over our previous paper [12] and focuses on the development of a *k*-distribution databasing scheme for the most significant species, atomic N and O.

2 Evaluation of Spectral Property of Gases

Radiation from atomic bound–bound lines makes far-and-away the most significant contribution to radiative heat flux for typical reentry conditions into earth's atmosphere; making bound-free, free–free, and diatomic radiation of lesser importance. This paper is an improvement over our previous paper [12] and utilizes state-of-the-art spectroscopic data taken from the National Institute of Standards and Technology (NIST) [13]. In the old paper, the spectroscopic constants were taken from the database of Sohn et al., which is derived from NEQAIR96 and comprises a total of 170 lines for N and 86 lines for O [14,15]. These data are vastly outdated and have been proven to lead to significant errors. Park [16] included the extended atomic line data in the NEQAIR code to perform radiation calculations for Fire II and Apollo 4 vehicles. He concluded that inclusion of new atomic lines from extended NIST data significantly increased the radiative intensity. An update of the NEQAIR code was presented by McCorkle et al. [17], using the extended atomic line data and updated Stark broadening database. Similar updated atomic and molecular data have been compiled by Chauveau et al. [18,19] and Johnston [20]. The updated spectroscopic data for the atomic bound–bound lines of N and O species used in the current work comprise 914 bound–bound lines for N and 682 for O for wavelengths below 20,000 Å [13]. Following the work of Sohn et al. [15], the spectroscopic constants from NIST were converted into a more efficient format for quick evaluation of absorption and emission coefficients. Following this format, absorption and emission coefficients for an isolated atomic bound–bound line can be written as

$$\varepsilon_\lambda(\underline{\phi}) = g_{e'} n'_e(\underline{\phi}) A_{e'e''} hc \frac{1}{\lambda}\frac{1}{4\pi}\Phi_\lambda = n'_e(\underline{\phi})\varepsilon^c_\lambda \Phi_\lambda \tag{1}$$

and

$$\kappa_\lambda(\underline{\phi}) = (n''_e(\underline{\phi}) - n'_e(\underline{\phi}))g_{e'}\frac{\lambda^4}{8\pi c}A_{e'e''}\Phi_\lambda = (n''_e(\underline{\phi}) - n'_e(\underline{\phi}))\kappa^c_\lambda\Phi_\lambda \tag{2}$$

where ε^c_λ and κ^c_λ are the constant part of the spectral emission and absorption coefficient (precalculated values stored in tables), Φ_λ is the Voigt line profile, and n'_e and n''_e are the populations of upper and lower nondegenerate electronic states, respectively. Under nonequilibrium, the gas state vector $\underline{\phi} = (T, T_e, \underline{n})$ depends on two temperatures—the translation temperature T and the electron temperature T_e—and the number density vector $\underline{n}$, specifying concentrations (of neutral, ion and electron). The database of Sohn et al. uses the Quasi-steady-state model (QSS) developed by Park [21] to model the nonequilibirum electronic state populations. This model groups all the electronic states into a total of 22 energy levels for N and 19 levels for O [15,21]. The Park model has been observed to lead to spurious inversions in electronic state populations. This discrepancy has been found largely due to outdated rate coefficients used in the QSS calculations. Therefore, the simplified interpolation tables for QSS calculations generated by Sohn et al. needed significant improvements. We collected state-of-the-art rate parameters from various references given by Johnston et al. and regenerated the interpolation tables from which electronic state populations of N and O can be calculated very efficiently through interpolation and lookup. These interpolation tables have been proven to be more efficient than the direct matrix inversion required in the QSS calculation. The new electronic excitation model employs 35 levels for N and 32 levels for O.

The Voigt profile Φ_λ is defined by Lorentzian and Gaussian line half-widths. The line width is an important parameter as it specifies how far from the line center a line retains its strength before its contribution becomes insignificant. Usually, with a Voigt line profile a strong atomic line may remain important up to 25–50 line half-widths on each side of the line, since it is optical thicknesses of order unity that contribute most to the radiative transfer. The Lorentzian width depends on a number of broadening mechanisms. For the case of high-temperature plasmas having high electron number densities, the Lorentz width is essentially governed by Stark broadening, while the Gaussian width comes from Doppler broadening. The Stark width b_S and Doppler width b_D can be written as [22]

$$b_S = b_{S,\text{ref}}\left(\frac{T_e}{T_{\text{ref}}}\right)^{0.33}\frac{n_e}{n_{e,\text{ref}}} = b_{S,\text{ref}}\varphi(n_e, T_e) \tag{3}$$

$$b_D = \lambda_\ell\sqrt{\frac{2k_B T \ln 2}{mc^2}} \tag{4}$$

where $b_{S,\text{ref}}$ is a reference Stark width value at a reference electron temperature of $T_{\text{ref}} = 10{,}000$ K, and reference electron density $n_{e,\text{ref}} = 10^{16}$ cm^{-3}; λ_ℓ is the wavelength at the center of an atomic line and m is the mass of the radiating atom. The dependency of the Stark width on n_e and T_e can be combined into a single normalized dimensionless parameter $\varphi(n_e, T_e)$. Thus, the Voigt line profile Φ_λ depends on two parameters, T and φ.

The RTE for an absorbing and emitting nonequilibrium hypersonic plasma can be written in a similar fashion to the equilibrium case [23] as

$$\frac{dI_\lambda}{ds} = \varepsilon_\lambda(\underline{\phi}) - \kappa_\lambda(\underline{\phi})I_\lambda = \kappa_\lambda(\underline{\phi})[I^{ne}_{b\lambda}(\underline{\phi}) - I_\lambda] \tag{5}$$

where $I^{ne}_{b\lambda}(\underline{\phi})$ is a nonequilibrium Planck function. The nonequilibrium Planck function is not a continuous function but rather is defined separately for each line at line center. In general, for an isolated line, the nonequilibrium Planck function can be written as

$$I^{ne}_{b\ell\lambda} = \frac{2hc^2}{\lambda^5_\ell}\left(\frac{n'_e}{n''_e - n'_e}\right) \tag{6}$$

The dependence of gas spectral properties on nonequilibirum QSS population makes databasing of these properties impractical, as it would require huge storage space in addition to fifth-order interpolation. It is imperative to define alternative gas properties independent of $\underline{\phi}$ before generating any meaningful database. If the spectrum is broken into a number of scales such that within each scale all overlapping atomic lines over a part-spectrum have similar dependency on n'_e and n''_e, the dependencies on $\underline{\phi}$ can be factored out and the number of parameters to database can be reduced. The stimulated emission term in the expression of absorption coefficient in Eq. (9) is approximated by assuming that the upper state population n'_e is related to the lower state population n''_e with a Boltzmann distribution at the free electron temperature T_e. In this way, the absorption coefficient can be approximated as

$$\kappa_\lambda(\underline{\phi}) = n''_e(\underline{\phi})\left(1 - \exp\left[\frac{-hc}{kT_e}(E_{e'} - E_{e''})\right]\right)\kappa^c_\lambda\Phi_\lambda(T,\varphi) = n''_e(\underline{\phi})\left(1 - \exp\left[\frac{-hc}{\lambda kT_e}\right]\right)\kappa^c_\lambda\Phi_\lambda(T,\varphi) \tag{7}$$

where $E_{e''}$ and $E_{e'}$ represent energy of upper and lower electronic states of the transition. The only QSS-dependent quantity in the above expression is n''_e, which is factored out and an absorption cross-section is defined as

$$\kappa'_\lambda(\underline{\psi}) = \frac{\kappa_\lambda}{n''_e} = \left(1 - \exp\left[\frac{-hc}{\lambda k T_e}\right]\right)\kappa^c_\lambda \Phi_\lambda(T, \varphi) \tag{8}$$

where $\underline{\psi}(T, T_e, \varphi)$ is the reduced gas state vector, which depends on three parameters as apposed to $\underline{\phi}$ that depends on five parameters (including number density of neutral atoms and ions) through the QSS model. For a group of overlapping lines, the absorption cross-section can be written as

$$\kappa'_\lambda(\underline{\psi}) = \sum_\ell \kappa^c_{\lambda,\ell}\left(1 - \exp\left[\frac{-hc}{\lambda k T_e}\right]\right)\Phi_{\lambda,\ell}(T, \varphi), \tag{9}$$

where the summation is taken over all bound–bound lines contributing at any wavelength λ and with the same n''_e. Approximation of the nonequilibrium Planck function is a little more tricky. If the lines do not overlap then there is no problem, as the Planck function near a given line will be governed by its own nonequilibrium Planck function given by Eq. (6). In theory, however, lines are infinitely wide, and therefore, overlap is always there. For overlapping lines, the nonequilibrium Planck function can be written as the ratio of emission and absorption coefficients as

$$I^{ne}_{b\lambda} = \frac{\varepsilon_\lambda}{\kappa_\lambda} = \frac{\sum_\ell \varepsilon_{\lambda,\ell}}{\sum_\ell \kappa_{\lambda,\ell}} \tag{10}$$

If the overlapping lines involve very different energy states then the nonequilibrium Planck function will not be a smooth function, as shown in Fig. 1 for $n''_e = 1 \rightarrow n'_e = 5$ and $n''_e = 2 \rightarrow n'_e = 20$. However, separating the lines from different transitions into different scales and assuming that lines from different scales do not overlap, the Planck function can be approximated as a smoothly varying function over each scale. For the m-th scale this is assumed as

$$I^{ne}_{bm\lambda}(\underline{\phi}) = I^c_{b\lambda} X_m(\underline{\phi}) \tag{11}$$

where

$$I^c_{b\lambda} = \frac{2hc^2}{\lambda^5} \tag{12}$$

and the parameter $X_m\left(\underline{\phi}\right)$ is calculated such that the total emission from the scale is conserved. The total emission from scale m can be written as

$$\varepsilon_m(\underline{\phi}) = \int_{\Delta\lambda} \varepsilon_{m\lambda}(\underline{\phi})d\lambda = n'_e(\underline{\phi}) \int_{\Delta\lambda} \varepsilon'_{m\lambda}(\underline{\psi})d\lambda \tag{13}$$

which can also be written as

$$\varepsilon_m(\underline{\phi}) = \int_{\Delta\lambda} \kappa_{m\lambda}(\underline{\phi}) I^{ne}_{bm\lambda}(\underline{\phi})d\lambda = n''_e(\underline{\phi}) X_m(\underline{\phi}) \int_{\Delta\lambda} \kappa'_{m\lambda}(\underline{\psi}) I^c_{b\lambda} d\lambda \tag{14}$$

Comparing the two relations

$$X_m(\underline{\phi}) = \frac{n'_e(\underline{\phi})}{n''_e(\underline{\phi})} \frac{\int_{\Delta\lambda} \varepsilon'_{m\lambda}(\underline{\psi})d\lambda}{\int_{\Delta\lambda} \kappa'_{m\lambda}(\underline{\psi}) I^c_{b\lambda} d\lambda} \tag{15}$$

3 Multiscale Part-Spectrum k-Distributions

In k-distributions, the rapidly varying spectral absorption coefficient is reordered into a monotonically increasing function over a narrow-band, part-spectrum or full spectrum. Most of the k-distribution methods to date have been developed for the case of thermodynamic equilibrium, where the radiation field is represented by a single temperature. The formulation of the k-distribution method for nonequilibrium is a little more challenging than its equilibrium counterpart, as shown by Bansal et al. [9]. In this section, a more general formulation of the multiscale part-spectrum k-distribution method is presented.

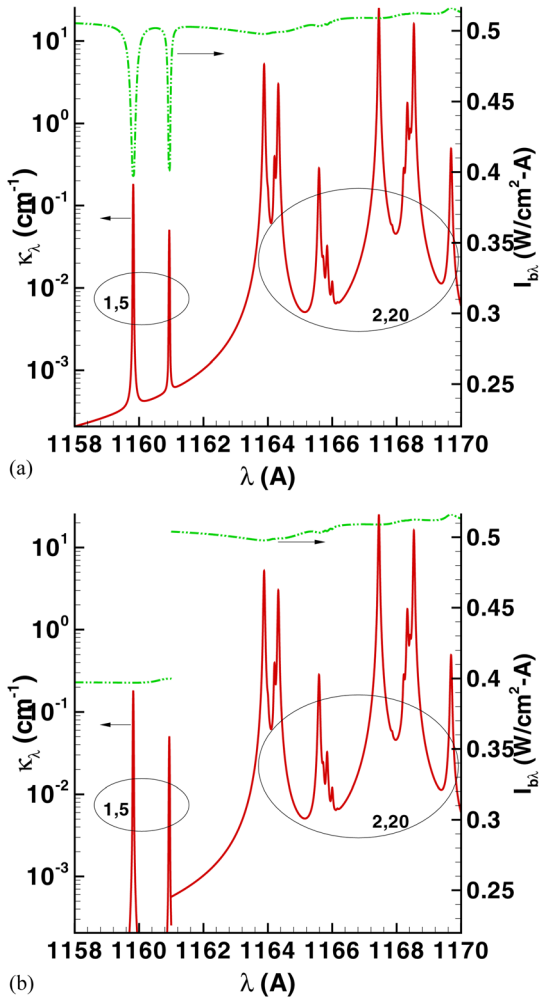

Fig. 1 Nonequilibrium Planck function (*a*) with overlap and (*b*) without overlap; $n_e = 5.0 \times 10^{15}$ cm^{-3}, $T_e = 10{,}000$ K, and $T = 15{,}000$ K

Equation (5) is reordered into a k-distribution by multiplying it with the Dirac-delta function $\delta(k_m - \kappa_{m\lambda}(\underline{\phi}_0))$, followed by integration over the part-spectrum, where $\kappa_\lambda(\underline{\phi}_0)$ is the absorption coefficient evaluated at some reference state $\underline{\phi}_0$. A part-spectrum is chosen in such a way that it covers atomic bound–bound lines belonging to the same scale (similar dependency on n'_e and n''_e) and satisfy the approximations made in Sec. 2. This leads to

$$\begin{aligned}\frac{dI_{km}}{ds} &= k^*_m(\underline{\phi}, k_m)\left[\int_{\Delta\lambda_m} I^{ne}_{bm\lambda}(\underline{\phi})\delta(k_m - \kappa_{m\lambda}(\underline{\phi}_0))d\lambda - I_{km}\right] \\ &= k^*_m(\underline{\phi}, k_m)[f_m(\underline{\phi}, \underline{\phi}_0, k_m) I^{ne}_{bm}(\underline{\phi}) - I_{km}]\end{aligned} \tag{16}$$

provided that every wavelength, where $\kappa_{m\lambda}(\underline{\phi}_0)$ has one and the same value k_m, $\kappa_{m\lambda}(\underline{\phi})$ also has one unique value $k^*_m(\underline{\phi}, k_m)$. In the above equation, f_m is the part-spectrum k-distribution for scale m, evaluated as

$$f_m(\underline{\phi},\underline{\phi}_0,k)=\frac{1}{I^{ne}_{bm}(\underline{\phi})}\int_{\Delta\lambda_m} I^{ne}_{bm\lambda}(\phi)\delta(k_m-\kappa_{m\lambda}(\phi_0))d\lambda$$
$$=\frac{1}{I^{ne}_{bm}(\underline{\phi})}\sum_i I^{ne}_{bm\lambda i}(\underline{\phi})\left|\frac{d\lambda}{d\kappa_{m\lambda}}\right|_{\kappa_{m\lambda}(\underline{\phi}_0)=k_m} \tag{17}$$

where summation is over all occurrences, $\kappa_{m\lambda}(\underline{\phi}_0)=k_m$. Using Eqs. (8) and (11)

$$f_m(\underline{\phi}_0,k_m)=\frac{1}{I^c_{bm}}\sum_i I^c_{b\lambda}\frac{1}{n''_e(\underline{\phi}_0)}\left|\frac{d\lambda}{d\kappa'_{m\lambda}}\right|_{\kappa'_{m\lambda}(\underline{\psi}_0)=k'_m}$$
$$=\frac{1}{n''_e(\underline{\phi}_0)}f'_m(\underline{\psi}_0,k'_m) \tag{18}$$

where f'_m is the k-distribution for the absorption cross-section $\kappa'_{m\lambda}$. Note that the quantity $X(\underline{\phi})$ cancels out, and therefore, dependency of f_m on gas state $\underline{\phi}$. Dividing Eq. (16) by $f_m(\underline{\phi}_0,k_m)$ leads to

$$\frac{dI_{gm}}{ds}=k^*_m(\underline{\phi},g_m)[I_{bm}(\underline{\phi})-I_{gm}] \tag{19}$$

where the cumulative k-distribution for the scale m can be defined as

$$g_m(\underline{\phi}_0,k_m)=\int_{k_m}^{\infty} f_m(\underline{\phi}_0,k_m)dk_m$$
$$=\frac{1}{n''_e(\underline{\phi}_0)}\int_{k_m}^{\infty} f'_m(\underline{\psi}_0,k'_m)dk'_m n''_e(\underline{\phi}_0)$$
$$=g'_m(\underline{\psi}_0,k'_m) \tag{20}$$

Since $k_m(\underline{\phi})$ and $k'_m(\underline{\psi})$ differ by only a constant factor, the cumulative k-distribution remains the same. Also, for numerical precision reasons a monotonically *decreasing* cumulative distribution is defined, as most of a full-spectrum k-distribution lies in the g-range $0\le g\le 0.01$.

In Fig. 2, sample k-distributions (k'_m versus g'_m) are plotted for selected scales of N and O. These k-distributions are plotted for the absorption cross-section $\kappa'_{m\lambda}$, and the actual k-distribution of a species can be constructed by scaling the k'_m values as

$$k_m(\underline{\phi},g_m)=n''_e(\underline{\phi})k'_m(\underline{\psi},g'_m) \tag{21}$$

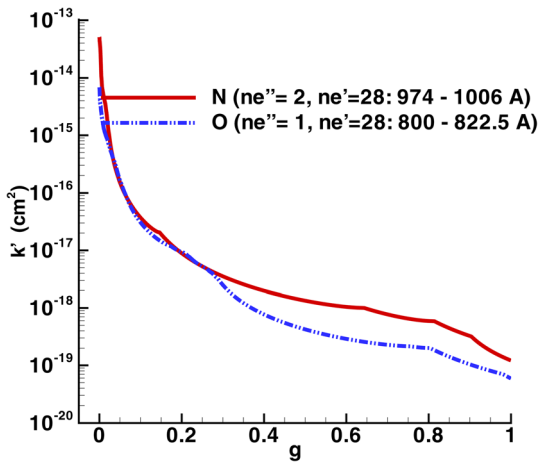

Fig. 2 Sample part-spectrum *k*-distributions; $n_e=5.0\times10^{15}$ cm^{-3}, $T_e=10{,}000$ K, and $T=15{,}000$ K

4 Assembly of Full-Spectrum *k*-Distributions From Part-Spectrum *k*-Distributions

Bansal et al. [9] have shown how the full-spectrum correlated-k distribution method can be applied to the atomic radiation transfer problem in hypersonic nonequilibrium flows. It has been demonstrated by Modest and Riazzi [10] that the required full-spectrum k-distributions can be assembled very quickly from a narrow-band database for any arbitrary gas state. If part spectra of scales of atomic bound–bound lines are assumed to be nonoverlapping, then the necessary full-spectrum k-distributions can be assembled in a method similar to developed by Modest and Riazzi. Equation (5) is multiplied by the Dirac-delta function $\delta(k-\kappa_\lambda(\underline{\phi}_0))$ and integrated over the full spectrum. This leads to

$$\frac{dI_k}{ds}=k^*(\underline{\phi},k)\left[\int_0^{\infty} I^{ne}_{b\lambda}(\underline{\phi})\delta(k_m-\kappa_\lambda(\underline{\phi}_0))d\lambda-I_k\right]$$
$$=k^*(\underline{\phi},k)[f(\underline{\phi},\underline{\phi}_0,k)I^{ne}_b(\phi)-I_k] \tag{22}$$

where

$$f(\underline{\phi},\underline{\phi}_0,k)=\frac{1}{I^{ne}_b(\underline{\phi})}\int_0^{\infty} I^{ne}_{b\lambda}(\phi)\delta(k-\kappa_\lambda(\phi_0))d\lambda$$
$$=\sum_{m=1}^{M}\frac{1}{I^{ne}_b(\underline{\phi})}\int_{\Delta\lambda_m} I^{ne}_{bm\lambda}(\phi)\delta(k-\kappa_{m\lambda}(\phi_0))d\lambda$$
$$=\frac{1}{I^{ne}_b(\underline{\phi})}\sum_{m=1}^{M} I^{ne}_{bm}(\underline{\phi})f_m(\underline{\phi},\underline{\phi}_0,k) \tag{23}$$

Equation (23) is a general relation for the assembly of part-spectrum k-distributions. One can either combine all the part-spectrum k-distributions into a full-spectrum k-distribution or one can combine different subsets of part-spectrum k-distributions to develop multigroup k-distributions. The reader is referred to our earlier work for more details [9]. Equation (22) can be transformed into the much smoother g-space by dividing it by the k-distribution at the reference state, $f(\underline{\phi}_0,\underline{\phi}_0,k)$, leading to

$$\frac{dI_g}{ds}=k^*(\underline{\phi}_0,\underline{\phi},g)[a(\underline{\phi},\underline{\phi}_0,g)I^{ne}_b(\underline{\phi})-I_g] \tag{24}$$

with

$$I_g=I_k/f(\underline{\phi}_0,\underline{\phi}_0,k) \tag{25}$$

$$I^{ne}_b(\underline{\phi})=\sum_{m=1}^{M} I^{ne}_{bm}(\underline{\phi}) \tag{26}$$

Here $k^*(\underline{\phi}_0,\underline{\phi},g)$ is the (k versus g) distribution with the absorption coefficient evaluated at the local conditions $\underline{\phi}$ and the Planck function at the reference state $\underline{\phi}_0$ [3], and $a(\underline{\phi},\underline{\phi}_0,g)$ is a weight or nongray stretching function given by

$$a(\underline{\phi},\underline{\phi}_0,g)=\frac{f(\underline{\phi},\underline{\phi}_0,k)}{f(\underline{\phi}_0,\underline{\phi}_0,k)}=\frac{dg(\underline{\phi},\underline{\phi}_0,k)}{dg(\underline{\phi}_0,\underline{\phi}_0,k)} \tag{27}$$

where

$$g(\underline{\phi},\underline{\phi}_0,k)=\int_k^{\infty} f(\underline{\phi},\underline{\phi}_0,k)dk=\sum_{m=1}^{M}\frac{I^{ne}_{bm}(\underline{\phi})}{I^{ne}_b(\underline{\phi})}\int_k^{\infty} f_m(\underline{\phi}_0,k)dk$$
$$=\frac{1}{I^{ne}_b(\underline{\phi})}\sum_{m=1}^{M} I^{ne}_{bm}(\underline{\phi})g_m(\underline{\phi}_0,k) \tag{28}$$

Table 1 Datapoints for the part-spectra database

Parameter	Range	Number
$T(K)$	2000–40000[a]	26
$T_e(K)$	2000–40000($T_e > T$)	26
φ (–)	1.0×10^{-3} –10.0	52
Part-spectra	N	30
	O	35

[a]Parameter values are chosen according to power law $\Delta T^{0.1}$=const, etc.

5 Database Generation

The main objective of this work is to generate and store accurate part-spectrum k-distribution $(k'_m(\underline{\psi}, g'_m))$ data as a function of the reduced gas state vector $\underline{\psi}(T, T_e, \underline{\phi})$. The gas state conditions used to generate the k-distributions are given in Table 1. It was found that more points are required for smaller values of all the parameters, for which the line shape tends to be narrower. To allow for efficient search-free retrieval, this is achieved by selecting equally spaced points along a power law distribution. The absorption cross-section has very strong dependence on the Stark width parameter φ, and thus relatively many φ points are needed in the database. Since the translational temperature T is always larger than the electron temperature T_e, the database comprises only those states for which $T > T_e$.

As a first step, lines of a species are sorted according to electronic states e' and e'' associated with the transition. After this initial sorting of lines, scales or groups of lines are formed such that each scale contains only those lines that have similar dependence on the electronic states. In this way, a total of 30 part-spectrum scales were created for N and 35 for O. Next, high-fidelity absorption cross-section data are generated for each part-spectrum with a spectral resolution of 0.001Å to ensure that generated k-distributions are accurate. From the high accuracy absorption cross-section data, k-distributions were generated for each of the gas conditions listed in Table 1. This involves choosing a (large) number of k'_m-bins and calculating the cumulative k-distribution $g'_m(\underline{\psi}, k'_m)$ for every k'_m-value. We employed 5000 k'-bins again distributed according to a power law distribution [11]. A k-distribution database employing 5000 points requires vast storage space −92 GB for all the conditions given in Table 1. Therefore, the next step is to reduce its size, without compromising accuracy. Wang and Modest [11] have described a number of schemes by which the size of the data can be reduced. This includes the concept of fixed g and storing the data using a Gaussian quadrature scheme. The k-distribution data are sets of k'_m-values for sets of g'_m-values, but not both need to be stored. One may fix either k'_m or g'_m-values for all part-spectra and only the other set of values needs to be in the database. Since the g'_m values always vary between 0 and 1, it is more convenient to fix values of g'_m. On the other hand, k-distributions are generated for a chosen set of k'_m-values, interpolation of k'_m-values at fixed g'_m-values is required before storing them in the database.

Following the work of Wang and Modest [11], a scalable Gauss–Chebyshev quadrature scheme was used for data compaction. An n-node Gauss-quadrature scheme has $(2n-1)$-th order of accuracy. The fixed g'_m-values are chosen as the abscissas of the Chebyshev polynomial of the second kind $U_n(x)$. The use of the Gauss–Chebyshev quadrature scheme has the particular advantage of scalability, i.e., the lower rank quadrature is a subset of the next higher rank quadrature. In other words, for any given U_n, one can always find another U_m, whose zeroes include all the zeroes of U_n. In practice, if we have a 128-point quadrature, we can take every fourth point to use a 32-point quadrature, without any interpolation. In this work, the minimum number of quadrature points used is 32 and a maximum of 128-points were used to set the fixed g'_m-values. The Gauss–Chebyshev quadrature scheme puts more quadrature points at higher g'_m-values. As already mentioned, it is advantageous to define a monotonically decreasing cumulative k-distribution and thus to have more quadrature points at lower g'_m-values, i.e., higher k'_m-values. This can be achieved by employing a transformation as

$$g'_n = (1 - g_n)^{\alpha} \tag{29}$$

leading to modified quadrature weights

$$w'_n = \alpha w_n (1 - g_n)^{\alpha - 1} \tag{30}$$

A value of $\alpha = 2.0$ places more points at smaller g-values and has been used in this work. With this quadrature scheme, the total size of the database was reduced to about 300 MB for both the species.

6 Application of the Database

In this section, the methodology to assemble a full-spectrum k-distribution from the database is presented. First part-spectra k-distributions are calculated at a given gas state by interpolating between the stored data. This requires interpolation in three-dimensional space formed by the variables T, T_e, and φ. Since in the database, all k'_m-values are stored at fixed g_m-values, this requires interpolation of k'_m-values for each part-spectrum. A simple and efficient trilinear interpolation scheme is utilized, employing a $2 \times 2 \times 2$ interpolation domain. All eight k-distributions in the interpolation domain must have the same number of points. Since, as a result of data compaction, different k-distributions may have different number of points (e.g., 32 for one and 64 for another), this may require an additional interpolation within individual k-distributions of all part-spectra. A cubic spline interpolation scheme is employed for this purpose. Once all part-spectrum k-distributions are known at a given gas state, the full-spectrum k-distribution can be assembled from the M part-spectra using Eq. (28). The addition in Eq. (28) is carried out at fixed k-values and requires another interpolation of $g_m(\underline{\phi}, k_m)$-values at fixed k-values for each part-spectrum. Again a cubic spline scheme is utilized to carry out this interpolation.

7 Sample Calculations

To check the accuracy of the database, a number of calculations were performed. First, the accuracy of each part-spectrum k-distribution was checked by comparing part-spectrum gas column emissivities $\bar{\epsilon}_m$, with those obtained from direct line-by-line calculations using

$$\bar{\epsilon}_m = \frac{1}{I^c_{bm}} \int_{\Delta\lambda_m} I^c_{b\lambda} (1 - e^{-\kappa'_\lambda n''_e L}) d\lambda = \int_0^1 (1 - e^{-k'_m n''_e L}) dg \tag{31}$$

where the values of $n''_e L$ is chosen in such a way as to provide an emissivity of approximately 0.40–−0.60, but restricting the maximum value to $n''_e L = 5.0 \times 10^{18}$ cm^{-2}, as larger values are unrealistic for general planetary entry conditions. Therefore, the actual emissivity value may not fall within the above specified range for all part-spectra. The accuracy was checked for a large number of interpolated states (a total of 10,000 randomly generated values of φ, T_e, and T), and the maximum relative error was found to be always below 0.5%, except for cases for which emissivity was very small. A typical calculation (for interpolated values of φ, T_e, and T) is shown in Fig. 3, where part-spectrum emissivities of a gas column containing atomic O are compared, showing excellent agreement with line-by-line results. Similar excellent agreement was obtained for N.

To demonstrate the accuracy of the k-distribution database when solving atomic radiation problems in hypersonic nonequilibrium flows, the k-distribution database is applied to calculate radiative heat transfer along the stagnation line of the Stardust vehicle shown in Fig. 4. Database results are compared with line-by-line results as well as with direct k-distribution results, where k-distributions are calculated on-the-fly from spectral absorption

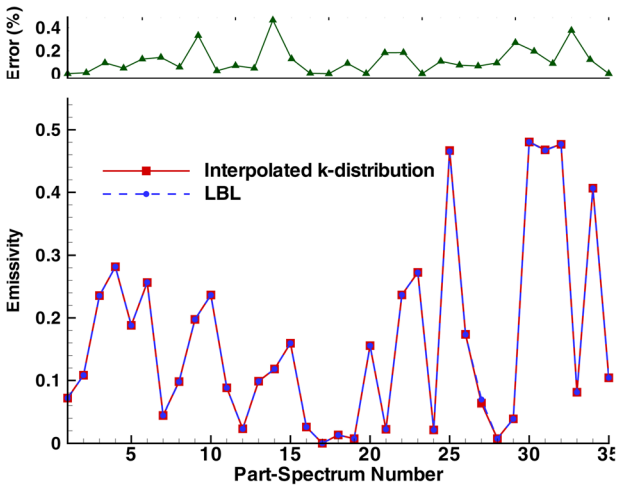

Fig. 3 Part-spectrum emissivity; $\varphi = .50$, $T_e = 10{,}000$ K, and $T = 15{,}000$ K

coefficient data. It has been shown that results obtained from the single group full-spectrum k-distribution method are relatively inaccurate compared with multigroup k-distribution results [9]. In the multigroup method, all the part-spectra are not combined into a single full-spectrum k-distribution, but rather a number of k-distributions are assembled from a subset of part-spectrum k-distributions and for each group RTEs are solved separately. Specifically,

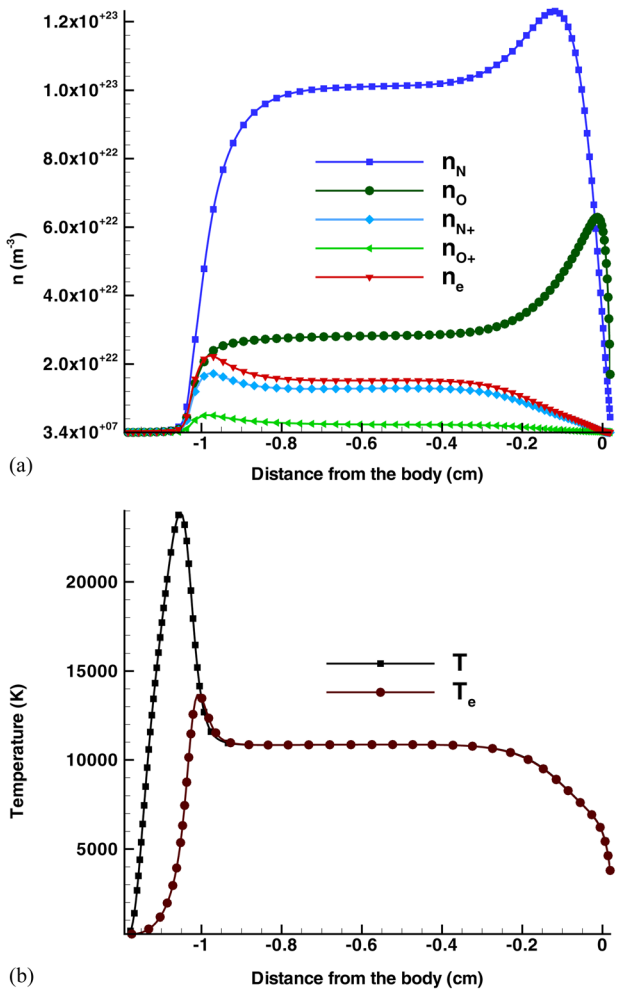

Fig. 4 Stardust stagnation line flow field (*a*) species number density and (*b*) temperature

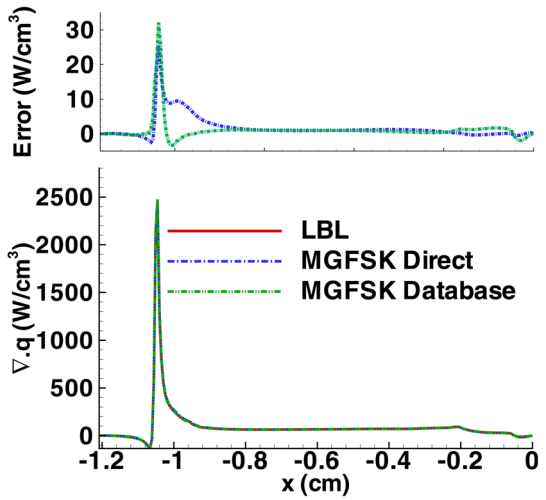

Fig. 5 Radiative heat source and absolute error along the Stardust stagnation line flow field

a 4-group model is employed in our calculations, as presented in our earlier work on the multigroup model [9]. Wall heat flux results obtained from both the direct 4-group FSK and database calculations agree to within 1% with the line-by-line results. In Fig. 5, results for divergence of heat flux are presented, demonstrating that very accurate results can be obtained using the database. The maximum absolute error in the radiative source term is about 30 W/cm^3 out of 2500 W/cm^3 in the overshoot region and about 2 W/cm^3 out of 70 W/cm^3 in the plateau region. The relatively larger error in the overshoot region is due to coarse resolution of the flow-field grid and the concentrated heat source.

8 Computational Efficiency

To demonstrate the efficiency of the k-distribution method together with the databasing scheme, computational times were measured for the heat transfer calculations for the Stardust stagnation line problem discussed above. The LBL method requires calculating emission and absorption coefficients at hundreds of thousands of wavelengths and solving the RTE at each of the wavelengths. The measured CPU-times for the LBL generation of spectral data and solution of the RTE are given in Table 2. Since time required in the LBL method directly depends on the spectral resolution at which spectral data are generated, results from two different resolutions are shown for comparison. In general, an atomic radiation calculation demands a resolution of at least 0.01 Å for good accuracy. At coarser resolutions, the accuracy of LBL results decreases. Errors as high as 6–7% in wall heat flux were observed for a resolution of 0.05 Å. Also, each line is assumed to be spread 50 Voigt line half widths on each side of the line center. The correlated-k method requires interpolation of spectral data at local gas conditions, assembly of full-spectrum k-distributions from the part-spectrum k-distributions, calculation of the a functions, and solution of the RTE at a number of quadrature points. The multigroup k-distribution model [9] was used for comparison.

Table 2 Computational time comparison (s)

	LBL spectral resolution (Å)	LBL data	LBL RTE	4-group FSK data	4-group FSK RTE
N	0.005	1476	14214	—	—
	0.01	398	6402	0.80	0.2
O	0.005	1031	13263	—	—
	0.01	327	6665	0.71	0.2
N + O	0.005	2470	14649	—	—
	0.01	648	7259	1.56	0.2

As many as 16 RTEs were solved for each group; 16×4 RTEs for four part-spectra groups.

All calculations were performed on a single Pentium-Xeon 3.0 GHz processor with cache size of 4 MB. In the k-distribution method, the database reading time is not included, as this is done only once and does not need to be repeated for each flow condition. The k-distribution method shows considerable savings in computational time for the generation of spectral data, as compared with the LBL data for both spectral resolutions (roughly by a factor of 10,000). The time saving is even more significant in the evaluation of the RTE, as the RTE is evaluated at only few quadrature points, compared with about 3×10^6 evaluations in the LBL method (approximately by a factor of 50,000). However, LBL calculations can be accelerated by a factor of about 10 choosing a variable grid spacing of wavelength points [24], which are still 5000 times more costly than the k-distribution method. Other higher order RTE solution methods for two- or three-dimensional geometries, e.g., the spherical harmonics and the discrete ordinate methods, are much more expensive than the tangent slab method, and one can expect enormous time savings when using k-distributions.

9 Conclusions

A multiscale part-spectrum k-distribution database for hypersonic nonequilibrium conditions has been developed for the two important monoatomic species N and O. The spectrum was broken up into 65 part-spectra according to the electronic states of transitions. High accuracy k-distributions were generated for each part-spectrum using high-fidelity absorption cross-section data. A Gauss–Chebyshev quadrature scheme was implemented for data compaction. The accuracy of the database was checked by comparing part-spectrum gas column emissivities with those obtained from line-by-line calculations, showing excellent accuracy. Finally, the database was applied to generate full-spectrum k-distributions, and heat transfer calculations were performed for the Stardust stagnation line flow-field, demonstrating that full-spectrum k-distributions can be assembled accurately from the part-spectrum k-distribution database. Computational times for the Stardust calculation showed significant reduction in the CPU time compared with line-by-line times for the evaluation of gas properties and solution of the RTE.

Nomenclature

A = Einstein coefficient for spontaneous emission, s^{-1}
c = speed of light, 2.9979×10^8 ms^{-1}
f = k-distribution, cm
f = normalized k-distribution, cm^{-2}
g = cumulative k-distribution
h = Planck's constant, 6.6262×10^{-34} Js
I = intensity, W/cm^2 sr
k = absorption coefficient variable, cm^{-1}
k = absorption cross-section variable, cm^2
M = total number of part-spectra
n, n = number density (vector), cm^{-3}
T = temperature, K

Greek Symbols

κ = absorption coefficient, cm^{-1}
κ' = absorption cross-section, cm^2
λ = wavelength, Å
$\underline{\phi}$ = gas state vector
$\overline{\Phi}$ = line shape function

Subscripts

b = blackbody
e = electron, electronic
g = at a given value of cumulative k-distribution
k = at a given value of reordered absorption coefficient
k' = at a given value of reordered absorption cross-section
ℓ = for a given atomic bound–bound line
m = for a given part-spectrum
λ = at a given wavelength

References

[1] Lacis, A. A., and Oinas, V., "A Description of the Correlated-k Distribution Method for Modeling Nongray Gaseous Absorption, Thermal Emission, and Multiple Scattering in Vertically Inhomogeneous Atmospheres," J. Geophys. Res., **96**(D5), pp. 9027–9063, doi:10.1029/90JD01945 (1991).

[2] Modest, M. F., and Zhang, H., 2002, "The Full-Spectrum Correlated-k Distribution for Thermal Radiation From Molecular Gas–Particulate Mixtures," ASME J. Heat Transfer, **124**(1), pp. 30–38.

[3] Modest, M. F., 2003, "Narrow-Band and Full-Spectrum k-Distributions for Radiative Heat Transfer—Correlated-k Versus Scaling Approximation," J. Quant. Spectrosc. Radiat. Transf., **76**(1), pp. 69–83.

[4] Rivière, P., Soufiani, A., and Taine, J., 1992, "Correlated-k and Fictitious Gas Methods for H_2O Near 2.7 μm," J. Quant. Spectrosc. Radiat. Transf., **48**, pp. 187–203.

[5] Rivière, P., Scutaru, D., Soufiani, A., and Taine, J., 1994, "A New c–k Data Base Suitable from 300 to 2500 K for Spectrally Correlated Radiative Transfer in CO_2–H_2O Transparent Gas Mixtures," In *Tenth International Heat Transfer Conference*, Taylor & Francis, pp. 129–134.

[6] Zhang, H., and Modest, M. F., 2002, "A Multi-Scale Full-Spectrum Correlated-k Distribution for Radiative Heat Transfer in Inhomogeneous Gas Mixtures," J. Quant. Spectrosc. Radiat. Transf., **73**(2–5), pp. 349–360.

[7] Zhang, H., and Modest, M. F., 2003, "Scalable Multi-Group Full-Spectrum Correlated-k Distributions for Radiative Heat Transfer," ASME J. Heat Transfer, **125**(3), pp. 454–461.

[8] Hermann, W., and Schade, E., 1971, "Radiative Energy Balance in Cylindrical Nitrogen Arcs," J. Quant. Spectrosc. Radiat. Transf., **12**(9), pp. 1257–1282.

[9] Bansal, A., Modest, M. F., and Levin, D. A., 2010, "Multigroup Correlated-k Distribution Method for Nonequilibrium Atomic Radiation," J. Thermophys. Heat Transfer, **24**(3), pp. 638–646.

[10] Modest, M. F., and Riazzi, R. J., 2005, "Assembly of Full-Spectrum k-Distributions from a Narrow-Band Database; Effects of Mixing Gases, Gases and Nongray Absorbing Particles, and Mixtures with Nongray Scatterers in Nongray Enclosures," J. Quant. Spectrosc. Radiat. Transf., **90**(2), pp. 169–189.

[11] Wang, A., and Modest, M. F., 2005, "High-accuracy, Compact Database of Narrow-Band k-Distributions for Water Vapor and Carbon Dioxide," J. Quant. Spectrosc. Radiat. Transf., **93**, pp. 245–261.

[12] Bansal, A., Modest, M. F., and Levin, D. A., 2009, "Narrow-Band k-Distribution Database for Atomic Radiation in Hypersonic Nonequilibrium Flows," ASME Paper No. HT2009-88120.

[13] Ralchenko, Yu., Kramida, A. E., and Reader, J., 2010, *NIST Atomic Spectra Database, Version 4*, National Institute of Standards and Technology (NIST), Physics Lab, available from http://www.nist.gov/pml/data/asd.cfm.

[14] Whiting, E., Park, C., Liu, Y., Arnold, J., and Paterson, J., 1996, "NEQAIR96, Nonequilibrium and Equilibrium Radiative Transport and Spectra Program: User's Manual," Nasa reference publication 1389, NASA/Ames Research Center, Moffett Field, CA.

[15] Sohn, I., Bansal, A., Levin, D. A., and Modest, M. F., 2010, "Advanced Radiation Calculations of Hypersonic Reentry Flows Using Efficient Databasing Schemes," J. Thermophys. Heat Transfer, **24**(3), pp. 623–637.

[16] Park, C., 2004, "Stagnation-Point Radiation for Apollo 4," J. Thermophys. Heat Transfer, **18**(1), pp. 349–357.

[17] McCorkle, E. R., Bose, D., and Hash, D. B., 2009, "Improved Modeling of Shock Layer Radiation in Air," AIAA Paper No. 2009-1028.

[18] Chauveau, S., Perrin, M. Y., Rivière, P., and Soufiani, A., 2002, "Contributions of Diatomic Molecular Electronic Systems to Heated Air Radiation," J. Quant. Spectrosc. Radiat. Transf., **72**, pp. 503–530.

[19] Chauveau, S., Deron, C., Perrin, M. Y., Riviere, P., and Soufiani, A., 2003, "Radiative Transfer in LTE Air Plasmas for Temperatures up to 15,000 K," J. Quant. Spectrosc. Radiat. Transf., **73**, pp. 113–130.

[20] Johnston, C. O., 2006, "Nonequilibrium Shock-Layer Radiative Heating For Earth and Titan Entry," Ph.D. thesis, Department of Aerospace Engineering, Virginia Polytechnic Institute and State University, Blacksburg, VA.

[21] Park, C., 1990, *Nonequilibrium Hypersonic Aerothermodynamics*, Wiley, New York.

[22] Hartung-Chambers, L., 1994, "Predicting Radiative Heat Transfer in Thermochemical Nonequilibrium Flow Fields," NASA Technical Memorandum 4564.

[23] Modest, M. F., 2003, *Radiative Heat Transfer*, 2nd ed., Academic, New York.

[24] Feldick, A. M., Modest, M. F., and Levin, D. A., "Closely Coupled Flowfield–Radiation Interactions During Hypersonic Reentry," J. Thermophys. Heat Transfer (in press).